Three-dimensional surface layer model for strong motion and liquefaction prediction

H. Takahashi [1], N. Fukuwa[2]

[1] *Associate Professor, Meijo University, hirohito@meijo-u.ac.jp*
[2] *Professor, Nagoya University, fukuwa@sharaku.nuac.nagoya-u.ac.jp*
…

Abstract

For predicting strong motion and liquefaction evaluation over a wide area, it is important to modeling 3D surface layer considered the spatial distribution of parameters (S-wave velocity, N-value, lithofacies) and a reproducibility of the dynamic characteristics. In this paper, we show the 3D surface layer model and strong ground motion and liquefaction prediction, using Nagoya City data as reference.

Modeling the 3D surface layer, we used the 34,600 points of borehole logs, the 499 points of PS logging and the 25,287 grain size analysis database. We classified lithofacies of borehole logs into seven strata. And we interpolated altitude values of stratum boundary. Using Kriging method as the interpolation algorithm, we modeled the stratum boundary at intervals of 50m grids according to latitude and longitude. And, we modeled cut/fill boundary data by calculating a difference among the DEM based on the latest topographic map and that of based on the 1940's aerial photograph and that of based on the old edition of topographic map at 1950's. In this way, we got the boundary grids of 8 strata. The lithofacies and N-values of borehole logs were interpolated for each stratum. The modeling procedure is as follows : 1) Depth of the descriptions of lithofacies and N-values in the borehole logs were standardized to obtain regularly aligned datasets for vertical intervals of 1m in the altitudes, 2) The values of lithofacies indexes were converted to grain size distribution (the composition ratio of gravel fraction, sand fraction and fine fraction) based on the grain size analysis database. 3) The irregularly scattered values of grain size distribution and N-values were horizontally interpolated to obtain regularly gridded datasets in each altitude, 4) The datasets were stacked vertically. 5) The values of grain size distribution at every grid were converted to the values of lithofacies indexes. The 3D lithofacies and N-value model shows good agreement with the geological profile from geotechnical engineering maps. The 3D lithofacies and N-value model was converted to 3D S-wave velocity structure model, using empirical conversion formula of S-wave velocity.

Using the 3D surface layer model, strong ground motions and liquefaction were simulated for the hypothetical Tonankai earthquake. The distribution of the simulated seismic intensity in Nagoya City area shows good agreement with that of observed building damage at Tonankai earthquake in 1944. Similarly, simulated distribution at "high" liquefaction potential shows good agreement with the liquefaction confirmed area at Tonankai earthquake in 1944.

Keywords: Three-dimensional surface layer model, Strong motion prediction, Liquefaction prediction

1. Introduction

Considering the earthquake disaster prevention measures of the city, it is important that the damage estimates for scenario earthquake is properly calculated. It is concerned in Nagoya City that serious damage would be caused by the huge earthquake in the Nankai Trough. Among many Japanese municipality, as the damage estimate investigation, strong motion prediction is often performed by the waveform simulation. For this reason, it is necessary to model properly surface layer around the city for strong motion and liquefaction prediction. The point to note in the modeling is twofold. One is a spatial distribution of S-wave velocity and lithofacies, and another is a reproducibility of the dynamic characteristics of the ground.

Fig.1 shows the geomorphologic classification map. Nagoya area is classified into three terrains (the eastern hills, the central plateau and the western plains). According to the geotechnical engineering map of Nagoya area [1], the underground has deposited since the pliocene is divided into 7 strata (AO, D4, D3U, D3L, DM, D1, PO). The surface layer is composed of D1 and PO in the eastern area, composed of D4, D3U, D3L and Dm in the central area, composed of AO, D3U, D3L and Dm in the western area, respectively (Fig.7). As parameters for estimating a value of S-wave velocity, N-value, depth, lithofacies and stratum are often used. In addition to strong motion prediction for evaluate of liquefaction, lithofacies and fine fraction are required. Therefore, it is necessary to estimate the 3D spatial distribution of N-values, lithofacies, and starata. As a method of estimating spatial distribution of N-values and lithofacies using borehole logs is proposed to be used (e.g. Eto et al., 2007 [2], Kimura et al., 2014 [3]). Because lithofacies is a character string data, it is impossible to apply a numerical interpolation method as N-values. So the interpolation method using the mode is generally applied for lithofacies. We suggest a new procedure to estimate the spatial distribution in the same interpolation method for N-value and lithofacies.

For waveform simulation, the surface layer models are required to reproduce the dynamic characteristics. In order to understand the dynamic characteristics at a number of sites widely spreading area, it is effective to use microtremour records. In Nagoya area, microtremour records were obtained at 340 sites, and compared to the dynamic characteristics, which is calculated by using the surface layer model.

In this paper, we show a 3D surface layer model for Nagoya area. And strong motion prediction and liquefaction evaluation were simulated by using surface layer model for scenario earthquake. The distribution of the seismic intensity and liquefaction points for 1944 Tonankai earthquake are compared to the predicted results to verify the surface layer model.

2. Surface Layer Modelling

2.1 Materials and Methods

The 3D surface layer model were constructed for an area of north-south 27km and east-west 28km, including Nagoya City and the altitude range from -150m to 150m. The models were constructed using a variety of materials - 34,600 points of borehole logs, 499 points of PS logging data, 25,287 samples of grain size analysis, the topographic map of 1950's and 2000's and aerial photographs shot by the GHQ. Fig.2 shows the distribution of borehole data in Nagoya City area. Survey points are shown in various colors depending on the digging length.

Firstly, we constructed cut/fill boundary data (BO) by calculating the difference between the DEM based on the latest topographic map (scale 1/2,500) and that of based on the old edition of topographic map at 1950's (scale 1/3,000). For areas where residential development had been carried out prior to the 1950s, DEM were created by photogrammetry based on the 1940's aerial photograph shot by the GHQ. Fig.3 shows the distribution of estimated Cut/Fill thickness. And, we classified lithofacies of borehole logs into eight strata - the reclamed layer (RO) was added to 7 layers according to the geotechnical engineering map [1]. And we interpolated altitude values of stratum boundaries. Using the kriging method as the interpolation algorithm, we modeled the stratum boundaries at intervals of 50m grids along both the north-south direction and the east-west direction. As an example, the distribution of the estimated basal surface of the AO layer in Fig.4. In this way, we got the boundary grids of 9 strata.

Secondly, based on the grain size analysis of 25,287 samples at 4,506 sites in Nagoya area, we have set the average grain size distribution for each lithofacies. At grain size distribution, similarly distributed lithofacies are merged. In triangular coordinates, the grain size distribution is shown for each index of lithofacies as an example in Fig.5. Filled circle shows the average value. Fig.5 shows that the grain size distribution of lithofacies, determined by the ground survey, shows varing widely. On the average, however, fine fraction of sandy clay is small compared to that of clay. Larger the N-value, higher the sand fraction. Table 1 shows the average value of the grain size distribution for each lithofacies and each stratum.

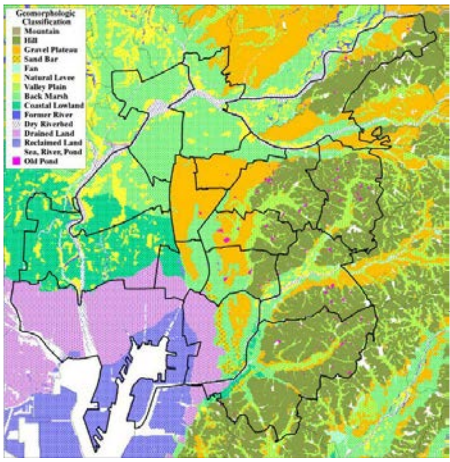

Fig.1 – The geomorphologic classification map in Nagoya area

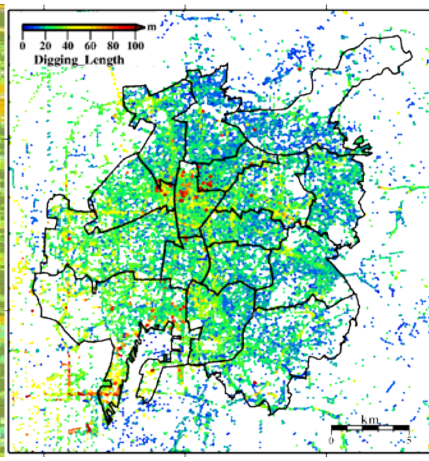

Fig. 2 – The distribution of borehole logs.

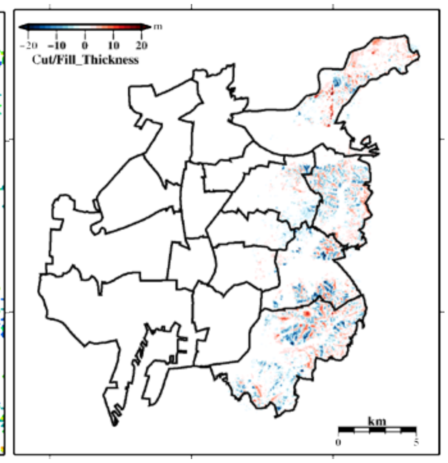

Fig. 3 – The distribution of estimated Cut/Fill thickness.

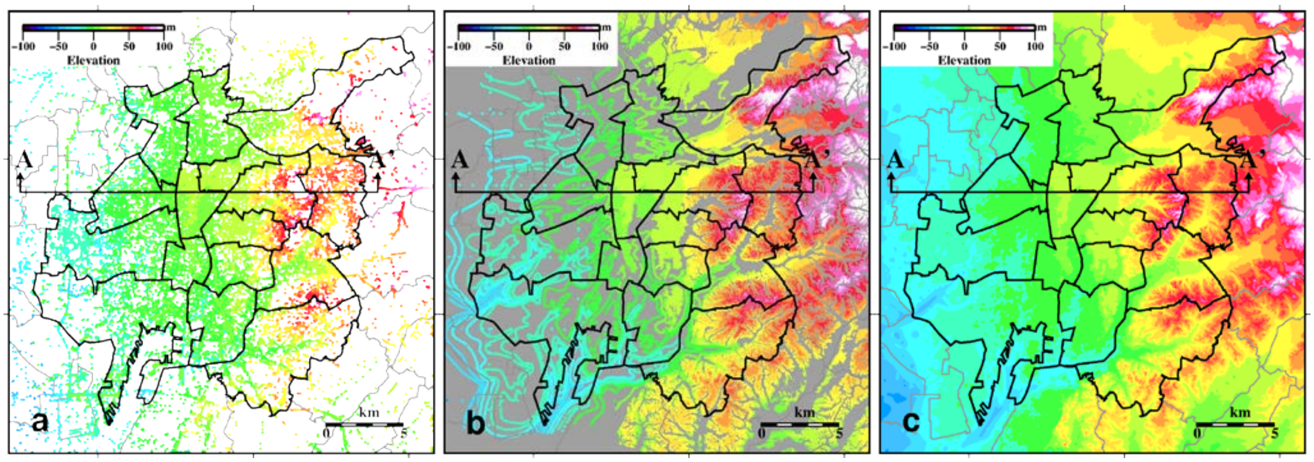

Fig. 4 – The distribution of the lower elevation of the AO layer from borehole logs (a), from the geotechnical engineering maps [1] (b) and from interpolated grid (c).

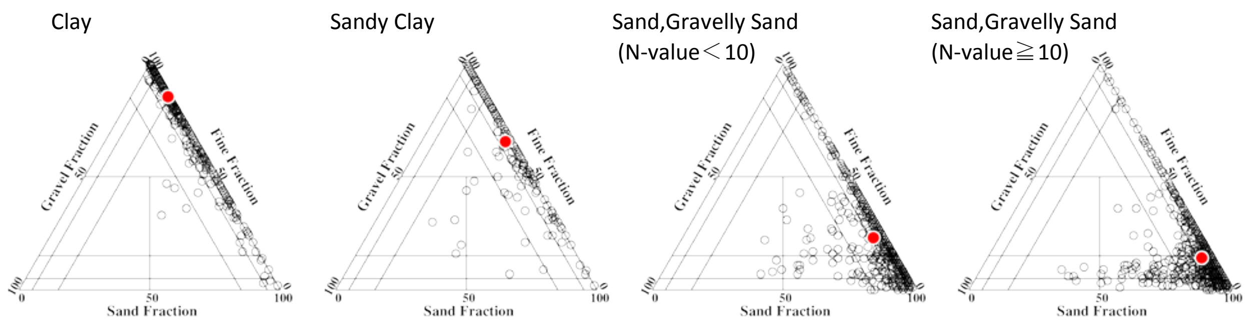

Fig. 5 –The grain size distribution is shown for each index of lithofacies in triangular coordinates as an example.

Table 1 – The values of grain size distribution for each lithofacies

Lithofacies	BO (Filled Layer)			RO (Reclaimed Layer)			AO		
	Gravel	Sand	Fine	Gravel	Sand	Fine	Gravel	Sand	Fine
Gravel	45.4	34.9	19.7	11.3	70.1	18.6	43.8	40.3	15.9
Sandy Gravel	–	–	–	–	–	–	45.6	39.5	14.9
Muddy Gravel	–	–	–	–	–	–	34.2	44.6	21.2
Sand (N<10)	7.0	69.1	23.9	2.1	81.0	16.9	2.7	65.9	31.4
Sand (N≧10)	3.4	79.3	17.3	2.4	87.4	10.2	3.0	78.5	18.5
Sand, Gravelly Sand (N<10)	8.3	73.8	17.9	2.1	86.8	11.0	3.9	73.1	23.1
Sand, Gravelly Sand (N≧10)	2.9	83.8	13.3	2.4	88.4	9.2	3.8	82.0	14.2
Muddy Sand (N<10)	5.6	64.1	30.3	1.8	59.8	38.4	2.2	63.1	34.7
Muddy Sand (N≧10)	4.3	71.4	24.3	2.8	73.1	24.1	1.8	73.1	25.0
Clay (Cohesive Soil)	5.0	14.5	80.5	0.6	18.3	81.1	0.8	22.0	77.2
Sandy Silt	4.0	38.0	58.0	2.6	41.4	56.0	1.4	35.8	62.8
Silt	1.7	20.5	77.8	0.2	15.1	84.7	0.5	16.8	82.7
Sandy Clay	9.5	35.4	55.2	2.0	27.4	70.5	2.2	32.1	65.6
Clay	1.8	11.5	86.7	0.1	10.9	89.0	0.3	14.2	85.5

Lithofacies	D4			D3U			D3L		
	Gravel	Sand	Fine	Gravel	Sand	Fine	Gravel	Sand	Fine
Gravel	54.7	33.8	11.5	44.6	41.7	13.7	45.8	31.8	22.4
Sandy Gravel	55.3	33.8	10.9	44.7	42.3	13.0	–	–	–
Muddy Gravel	42.7	34.3	23.0	43.3	37.2	19.5	–	–	–
Sand（N<10）	10.0	61.4	28.7	3.3	69.4	27.3	3.2	59.9	37.0
Sand（N≧10）				3.9	72.9	23.2			
Sand, Gravelly Sand (N<10)	12.6	65.4	22.0	3.9	73.7	22.4	2.7	70.2	27.2
Sand, Gravelly Sand (N≧10)				4.6	76.8	18.6			
Muddy Sand (N<10)	4.9	53.8	41.4	2.2	62.5	35.3	3.5	53.4	43.1
Muddy Sand (N≧10)				2.1	62.4	35.5			
Clay (Cohesive Soil)	2.7	18.3	79.0	1.0	24.4	74.7	0.3	16.9	82.8
Sandy Silt	1.2	18.0	80.8	0.8	29.4	69.7	0.5	25.5	74.0
Silt				0.7	20.6	78.7	0.2	14.9	84.9
Sandy Clay	5.2	18.6	76.2	2.1	33.2	64.7	0.8	33.2	66.0
Clay				1.0	19.8	79.2	0.3	11.8	87.9

Lithofacies	DM			D1			PO		
	Gravel	Sand	Fine	Gravel	Sand	Fine	Gravel	Sand	Fine
Gravel	45.9	39.7	14.3	48.1	32.2	19.7	44.7	38.6	16.7
Sandy Gravel	46.0	40.2	13.7	44.5	35.0	20.5	41.1	43.0	15.9
Muddy Gravel	44.9	35.3	19.8	48.8	31.7	19.5	47.4	35.3	17.3
Sand	2.9	66.6	30.6	12.3	58.6	29.1	5.7	63.8	30.6
Sand, Gravelly Sand	3.4	71.2	25.5	15.5	60.2	24.3	7.1	68.4	24.4
Muddy Sand	1.9	57.6	40.5	9.7	57.2	33.0	3.5	56.8	39.7
Clay (Cohesive Soil)	0.6	18.0	81.5	5.0	22.4	72.6	1.5	21.1	77.4
Sandy Silt	0.8	30.2	69.1	2.9	34.6	62.6	2.6	32.5	64.9
Silt	0.4	15.3	84.3	0.2	19.7	80.0	0.9	16.5	82.7
Sandy Clay	0.1	12.0	87.9	12.3	29.7	58.0	1.5	27.3	71.2
Clay	2.0	23.5	74.5	3.6	16.8	79.5	2.0	19.5	78.5

Thirdly, the lithofacies and N-values of borehole logs were interpolated for each stratum. The modeling procedure, according to Eto's procedure [2], is as follows : (1) Depth of the descriptions of lithofacies and N-values in the borehole logs were standardized to obtain regularly aligned datasets for vertical intervals of 1m in the altitudes. Lithofacies is represented by that of the thickest layer in altitude interval of 1m. (2) The values of lithofacies indexes were converted to the average value of the composition ratio of gravel fraction, sand fraction and fine fraction based on the grain size analysis database. (3) The irregularly scattered values of N-values and the composition ratio of gravel fraction, sand fraction and fine fraction were horizontally interpolated to obtain regularly gridded values at intervals of 50m along both the north-south direction and east-west direction for each altitude. Finding the sum of grain size composition for each grid after interpolation to 100%, triangulation with linear interpolation method was used. (4) The gridded datasets were stacked vertically. (5) The values of grain size distribution for each grid were converted to lithofacies as follows:

a) Clay: Fine fraction is 50% or more
b) Sand: Fine fraction is less than 50% and sand fraction is more than gravel fraction
c) Gravel: Fine fraction is less than 50% and gravel fraction is more than sand fraction

The values of the gray row in Table 1 were adopted representative values of gravel, sand and fine fraction.

2.2 Spatial Distribution of Lithofacies and N-value

Fig.6 shows examples of spatial distribution of lithofacies and N-values, as vertical cross section at A-A' line from constructed 3D models. The distribution of lithofacies corresponds with that of N-values, for example, N-value of clay grids is less than 10, and that of gravel grids is 50 or more. So we believe that spatial interpolation is appropriately done.

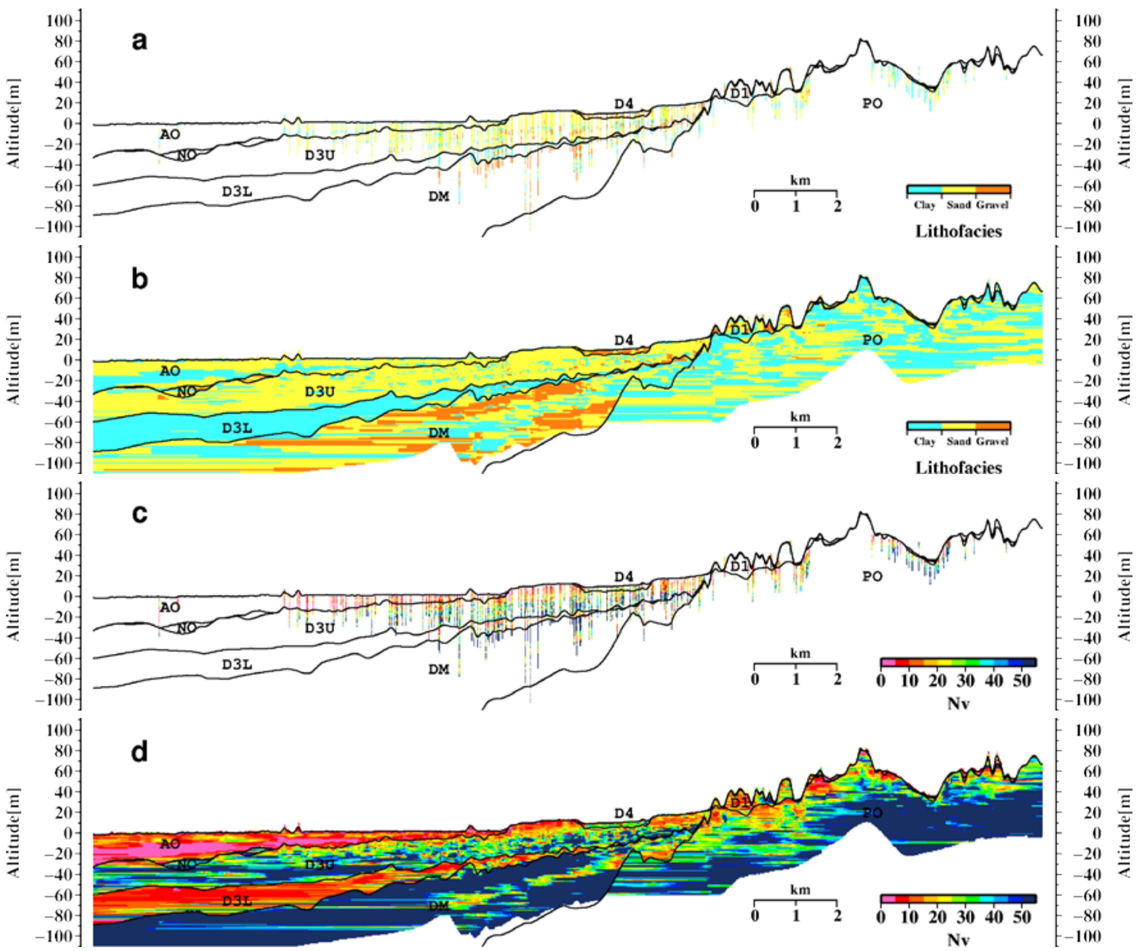

Fig. 6 – Borehole logs projected to A-A' line in the Fig.1 (a : lithofacies, c : N-values), and a cross section of lithofacies (b) and N-values (d) from constructed 3D models.

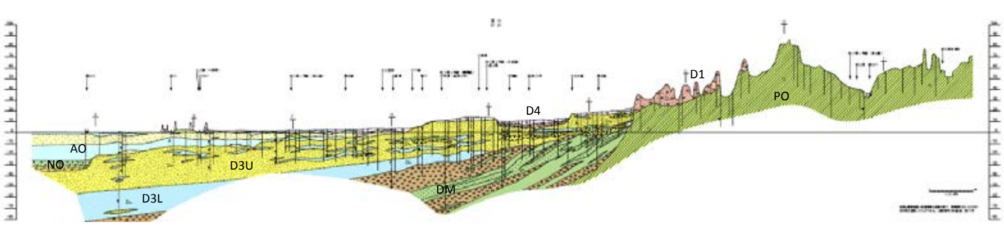

Fig. 7 – The geological profile from geotechnical engineering maps [1].

For comparison, Fig.7 shows the geological profile from geotechnical engineering maps [1]. Estimated spatial distribution of lithofacies from the models shows good agreement with the geological profile from geotechnical engineering maps. In general, the creation of geological profile is based on knowledges and judgments of engineers. Good correspondence between Fig.6 and Fig.7 indicates that the spatial distribution of lithofacies created by knowledges and judgements of engineers, have been objectively and appropriately estimated by modeling procedure applied in this study.

The deeper grids, the distributions of lithofacies and of N-value appear to be horizontally. This might be because the low number of borehole data with long digging length. In the tilted soil, like Nagoya City area, lithofacies and N-values should be modeled in the tilting direction. (Improvements of the interpolation procedure of data and the increase of borehole data are desired.)

2.3 Verification of Dynamic Characteristics

We convert the 3D grid model of N-values and Lithofacies to S-wave velocity structure model. The S-wave velocity estimation formula was constructed based on the PS logging data [4]. The estimation formula is as follows.

$$\mathrm{Log}V_s = C_0 + C_N\,\mathrm{Log}N + C_D\,\mathrm{Log}D + C_G + C_E \pm \sigma \tag{1}$$

V_s is S-wave velocity, N is N-value, D is the center depth of the layer, respectively. C_0, C_N, C_D, C_G, C_E are the regression coefficient, whose values shown in Table 2.

To evaluate constructed 3D S-wave velocity structure model applicable to Strong motion prediction, we compared dynamic characteristic with the observed records. There were 340 microtremour records in Nagoya area [5]. In this study, we picked up the 1D S-wave velocity structure models for each microtremour site to calculate the theoretical H/V spectrum [6]. Subsequently, we verified the model, comparing the observed H/V spectrum to the theoretical H/V spectrum. For calculating theoretical H/V spectrum, the subsurface structure model [7] was connected to under 3D S-wave velocity structure model. Fig.8 shows the distribution of predominant frequency based on the microtremour records.

Table 2 – The regression coefficients for estimating S-wave velocity

10^{C0}	C_N	C_D	10^{CG}				10^{CE}							
			Clay	Silt	Sand	Gravel	BO	AO	D4	D3U	D3L	DM	D1	PO
110.35	0.116	0.161	1.000	0.967	0.946	1.066	1.000	0.879	1.104	1.038	1.032	1.155	1.431	1.375

Generally, we focus on the shape of H/V spectrum at short period. The peak shape of H/V spectrum is obviously shown at the velocity structure having the boundary of layers where S-wave velocity contrast is high. On the other hand, the peak shape of H/V spectrum is not obviously shown at the velocity structure having the boundary of layers where S-wave velocity contrast is low, therefore there is difficulty when we evaluate using only predominant frequency.

So we evaluated S-wave velocity structure model comparing the shape between the observed H/V spectrum and theoretical H/V spectrum. The comparing sample is shown on Fig.9. On this sample, at the area where the peak shape of short period is obviously shown, we compared predominant frequency between the observed H/V spectrum and the theoretical H/V spectrum. Fig.8 shows compared predominant frequencies between the observed H/V spectrum and the theoretical H/V spectrum based on S-wave velocity structure model. Fig.10 shows good corresponding of predominant frequency between the observed and the theoretical H/V spectrum in short period.

According to the above results, the S-wave velocity structure model constructed is considered to be applicable to strong motion prediction for a wide area.

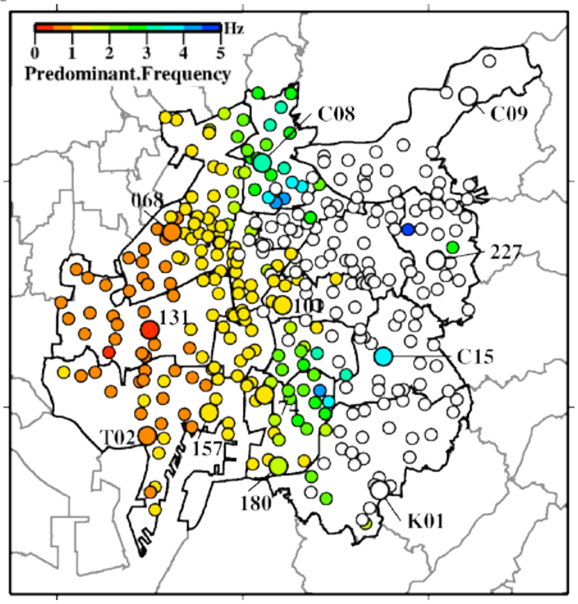

Fig. 8 – The distribution of predominant frequency based on the microtremour records.

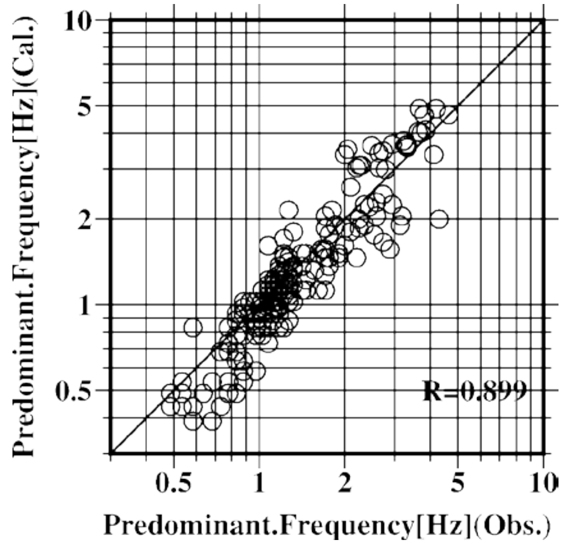

Fig. 10 – Comparison with the predominant frequency of the observed H/V spectra and that of the theoretical H/V spectra.

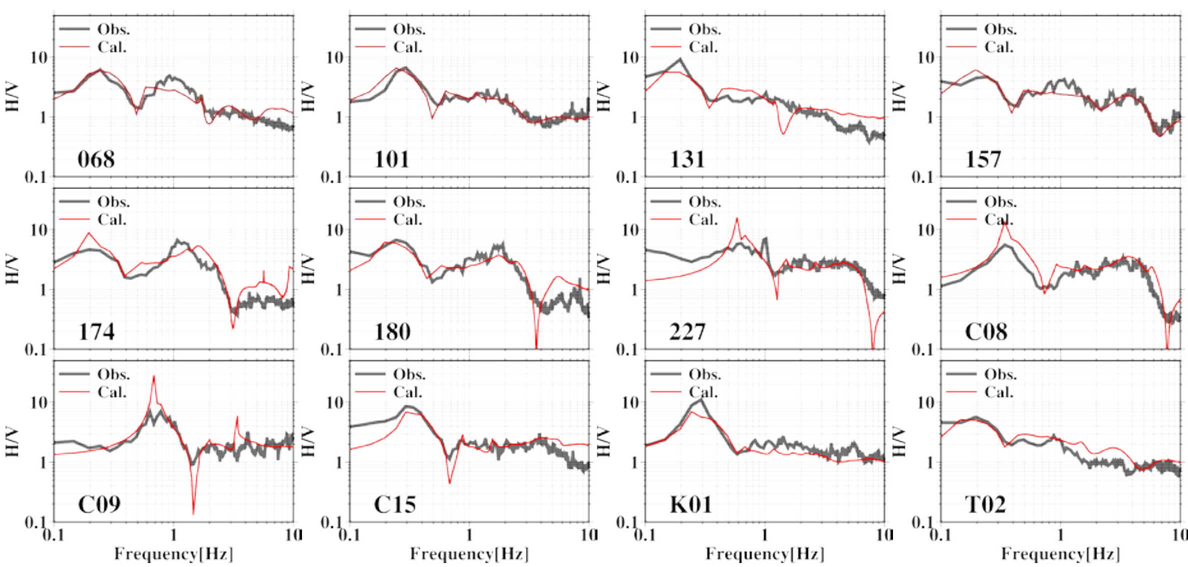

Fig. 9 – Examples of comparison between theoretical H/V spectra and observed H/V spectra based on microtrmour

3. Strong Motion and Liquefaction Prediction of the Hypothetical Tonankai Earthquake

3.1 Data and Analysis

We simulate the strong motion of the hypothetical Tonankai earthquake in the Nagoya City district. In this simulation, we used the source model of the hypothetical Tonankai earthquake by Cabinet Office [8]. The source model of the hypothetical Tonankai earthquake is shown in Fig.11. We use stochastic Green function method [9] on strong motion simulation from the source to the engineering bedrock. As the calculated method, we followed Cabinet Office [8] about Q value, shape of envelope, and site amplification at the subsurface structure model. During application of stochastic Green function, we assigned 10 patterns of fluctuation to rupture propagation using random numbers. Among calculated 10 patterns of distribution of seismic intensity at engineering bedrock, we picked up the cases which shows the average value of seismic intensity.

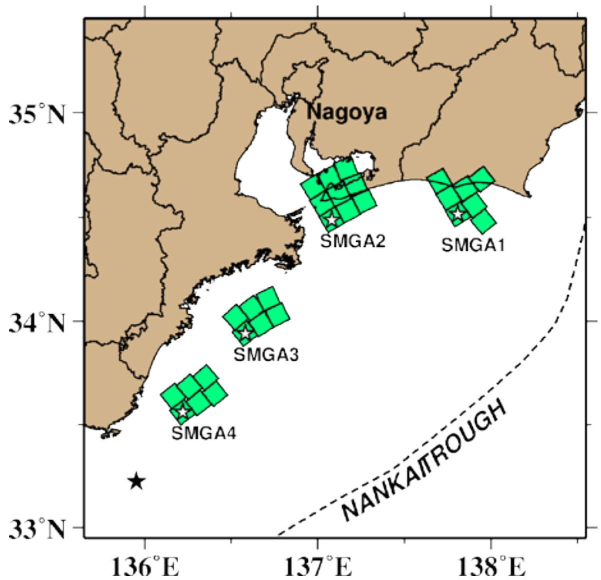

Fig. 11 – The source model of the hypothetical Tonankai earthquake [8]

Table 3 – The source parameters of the hypothetical Tonankai earthquake [8]

	SMGA1	SMGA2	SMGA3	SMGA4
Area (km^2)	713.3	913.5	613	615.8
Seismic Moment (Nm)	2.3×10^{20}	3.4×10^{20}	1.9×10^{20}	1.9×10^{20}
Moment Magnitude Mw	7.5	7.6	7.4	7.4
Stress Drop (MPa)	30	30	30	30
Rise Time (s)	4.9	5.6	4.6	4.6
Rupture Velocity (km/s)	2.7			
Fmax (Hz)	6			

As the seismic response analysis from engineering bedrock to surface, we adopted one of total stress non-linear analysis, DYNES3D [10]. About dynamic deformation characteristics, we used the average characteristic, which has been already estimated based on 213 samples at 42 sites in Nagoya City [11].

For evaluation of liquefaction was done based on PL-value, and we calculated FL for each layer, using the maximum shear stress calculated by total stress non-linear analysis.

3.2 Results and Discussion

Fig.12 shows calculated distribution of seismic intensity, using simulated waveform of surface for each grid. In this simulation, we calculated seismic intensity using Sakai's method [12] (hereafter, Ip), which is good corresponding to building damage. Fig.10 shows that the areas whose Ip is more than 5.5 would be mainly at around Nagoya port. Fig.13 shows the distribution of collapse rate of wooden houses for each Renku due to Tonankai earthquake in 1944 [13]. Fig.11 shows the confirmed house damage areas are limited within southeast in Nagoya City. And more, the areas whose collapse rate is more than 1% are limited within around Nagoya port, which is good agreement with the distribution of Ip (Fig.12).

Fig.14 shows the distribution of PL value evaluated by maximum shear stress calculated by the results of seismic response analysis. Fig.14 shows that the areas whose PL value is over 15 are distributed at around Nagoya port.

Fig. 15 shows the distribution of liquefaction areas and points caused by Tonankai earthquake in 1944 [14, 15]. Fig.15 shows the liquefaction areas and points are distributed at around Nagoya port, and it is good agreement with the areas whose PL values is over 15 at Fig.12. On the other hand, there is distribution of liquefaction areas and points in western area in Nagoya City, whose PL values is evaluated larger than the surrounding area.

The areas, whose house damage rate is larger, and liquefaction areas and points due to Tonankai earthquake in 1944, are good corresponding to the areas whose thickness of the AO layer is larger than surroundings (Fig.2). The simulation results is reflected by thickness of AO layer, in addition the spatial distribution of lithofacies and N-value, which indicates the application of the modeling procedure.

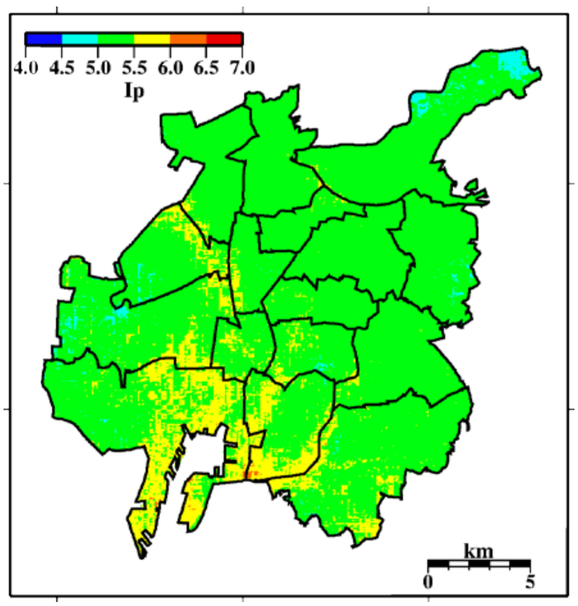

Fig. 12 – The distribution of simulated Ip.

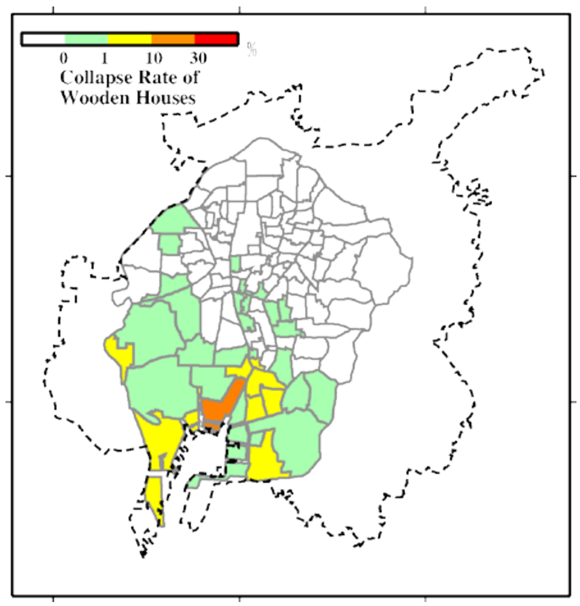

Fig. 13 – The distribution of collapse rate of wooden houses due to Tonankai earthquake in 1944.

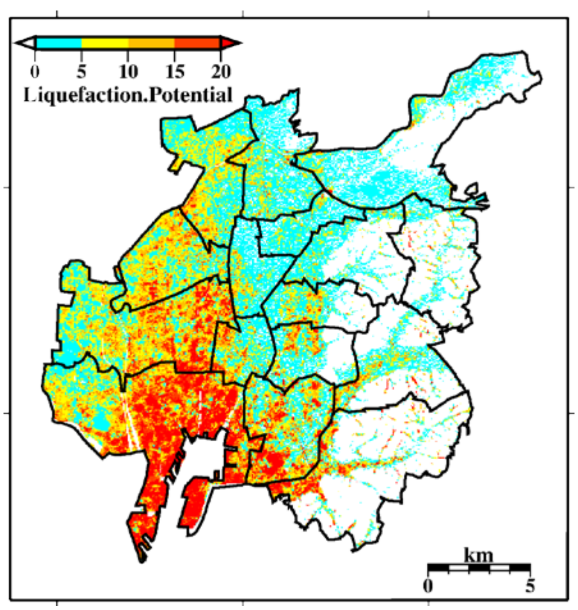

Fig. 14 – The distribution of PL-value.

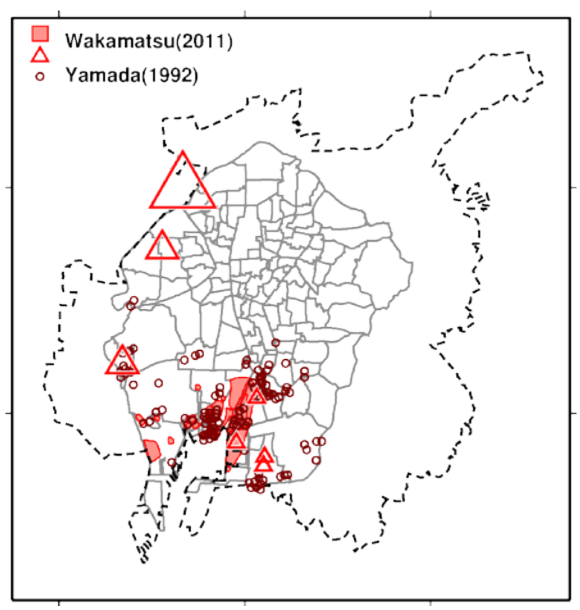

Fig. 15 – The distribution of liquefaction areas due to Tonankai earthquake in 1944.

4. Conclusion

In this study, 3D surface layer model is constructed in Nagoya area, then strong motion prediction and liquefaction evaluation are simulated for the hypothetical Tonankai earthquake.

(1) During spatial interpolation of lithofacies, we suggested the procedure that can interpolate numerically, the same as N-value. Lithofacies was quantified using grain size distribution. Then gravel fraction, sand fraction, and fine fraction are interpolated numerically.

(2) The spatial distribution of lithofacies from constructed 3D grid model is good agreement with the geotechnical engineering maps.

(3) The shape of spectrum in short period, it is good corresponding between the theoretical H/V spectrum based on the constructed model and the observed H/V spectrum based on microtremour records. About the predominant frequency in short period, it is good corresponding between the theoretical one and the observed one.

(4) It is good agreement at the distributions between the simulated Ip and damaged Renku of Tonankai earthquake in 1944. And, it is good agreement between the areas, whose PL value is over 15, and the distributions of liquefaction areas of Tonankai earthquake in 1944.

In this study, we simulated strong motion and liquefaction evaluation using 1D structure model extracted from each 50m grid of Nagoya area, in the directions of southnorth and eastwest. We would simulate in consideration of 3D heterogeneity influence using the constructed S-wave velocity structure model.

5. Acknowledgment

The authors wish to express their appreciation to Dr. Y. Sakai at Tsukuba University for providing the program of calculating seismic intensity, Ip. The surface layer model shown in this paper was created in the commission of Nagoya - "Survey for the damage estimation and disaster prevention and mitigation for the Tokai, Tonankai and Nankai earthquakes".

6. References

[1] Chubu Branch of the Japanese Geotechnical Society (1988): *Geotechnical Data of Subsoils in Nagoya, New Edition*, Publications Committee of Subsoils in Nagoya. (in Japanese)

[2] Eto, C., Ishihara, Y., Tanabe, S., Kimura, K., and Nakayama, T. (2007): Three-dimensional models of lithofacies and N-values of alluvial deposits obtained using borehole logs: An example of the latest Pleistocene to Holocene incised-valley fills in northern part of the Tokyo lowland, central Japan, *Journal of Sedimentological Society of Japan*, **64**, 9-13.

[3] Kimura K., Hanashima Y., Nishiyama S., Ishihara Y. (2014): Shallow-level subsurface three-dimensional geological modeling based on analysis of borehole data: A case of the northern Tokyo and the southern Nakagawa lowland area, *Integral research and application of the subsurface geology "the central Kanto Plain", Miscellaneous map series*, **40**, 56-113. (in Japanese with English Abstract)

[4] Takahashi H., Mori M. Fukuwa N. (2015): Study on Precision of the Estimated Average Shear-Wave Velocity based on PS Logging Data in Nagoya City Area, *AIJ Journal of Technology and Design*, **21**, 47, 375-380. (in Japanese with English Abstract)

[5] Nakamura H., Fukuwa N., Takahashi H., Tobita J., Hori K. (2000). A study on the characteristics of ground motion and the depth of seismological bedrock and engineering-basis bedrock in Nagoya city based on microtremor measurements, *Journal of structural engineering*, **46B**, 413-421. (in Japanese with English Abstract)

[6] Arai H., Tokimatsu K. (2004): S-Wave Velocity Profiling by Inversion of Microtremor H/V Spectrum, *Bulletin of the Seismological Society of America*, **94**, 1, 53-63.

[7] Horikawa H., Yoshimi M., Sekiguchi H., Yoshida K., Sugiyama Y., Satake K., Fukuwa N., Suzuki H., Matsuyama H., Liu Y., Takizawa F. (2008): A Three-dimensional Subsurface Structure Model of the Chukyo Area, Central Japan, *Annual report on active fault and paleoearthquake researches*, **8**, 47, 203-254. (in Japanese with English Abstract)

[8] Cabinet office Government of Japan (2015): Report on the long-period ground motion by the huge earthquake along the Nankai Trough. (in Japanese)

[9] Kamae K., Irikura K. (1994): Simulation of Seismic Intensity Distribution During the 1946 Nankai Earthquake Using a Stochastically Simulated Green's Function, *Proc. of 9th Japan Earthquake Engineering Symposium*, 1, 559-564.

[10] Yoshida N. (2006): DYNES3D A computer program for dynamic response analysis of level ground by effective stress-nonlinear method. (in Japanese)

[11] Takahashi H., Mori M., Noda T., Miyakoshi J., Tsuduki M., Fukuwa N. (2013): Nonlinear property for surface strata at Nagoya District, *Summaries of Technical Papers of Annual Meeting AIJ*, 253-254. (in Japanese)

[12] Sakai Y., Kanno T., Koketsu K. (2004): Proposal of Instrumental Seismic Intensity Scale from Response Spectra in Various Period Ranges, *Journal of Structural and Construction Engineering*, **585**, 71-76. (in Japanese with English Abstract)

[13] Iida K. (1974): Distribution of the earthquake damage caused by the Tonankai earthquake of December 7, 1944, *Past earthquakes and disasters in Nagoya City*, The Earthquake Section of Disaster Prevention Committee of Nagoya City, 42-78. (in Japanese)

[14] Wakamatsu K. (2011) : *Maps for historic liquefaction sites in Japan*, University of Tokyo Press. (in Japanese)

[15] Yamada K. (1992): Liquefaction Potential for the Alluvial Ground in Nagoya during the Predicted Earthquake, *Journal of Japan Society of Civil Engineers*, **445**, Ⅲ-18, 34-45. (in Japanese with English Abstract)